The Effect of Print Parameters on the (Micro) structure of 3D Printed Cementitious Materials

J. Van Der Putten(✉), G. De Schutter, and K. Van Tittelboom

Ghent University, Ghent, Belgium
jolien.vanderputten@ugent.be

Abstract. The extrusion-based 3D printing method is one of the main additive manufacturing techniques worldwide in construction industry. This method is capable to produce large scale components with complex geometries without the use of an expensive formwork. The main advantages of this technique are encountered by the fact that the end result is a layered structure. Within these elements, voids can form between the filaments and also the time gap between the different layers will be of great importance. These factors will not only affect the mechanical performance but will also have an influence on the durability of the components. In this research, a custom-made 3D printing apparatus was used to simulate the printing process. Layered specimens with 0, 10 and 60 min delay time (i.e. the time between printing of subsequent layers) have been printed with two different printing speeds (1.7 cm/s and 3 cm/s). Mechanical properties including compressive and inter-layer bonding strength have been measured and the effect on the pore size and pore size distribution was taken into account by performing Mercury Intrusion Porosimetry (MIP) tests. First results showed that the mechanical performance of high speed printed specimens is lower for every time gap due to a decreased surface roughness and the formation of bigger voids. The porosity of the elements shows an increasing trend when enlarging the time gap and a higher printing speed will create bigger voids and pores inside the printed material.

Keywords: 3D printing · Mechanical properties · Microstructure
Porosity · Pore size distribution

1 Introduction

In recent years, 3D printing of concrete has become one of the emerging technologies that can minimize the supply chain in the construction process by automatically producing building components with complex geometries layer by layer, directly from a digital model without human intervention [1, 2]. Hence to some extent, it could save material wastage, construction time and manpower. This new construction technique shows many advantages, but also has to challenge a couple of dualities compared to traditional casted concrete. First, the material has to be fluid to prevent any blocking or segregation during extrusion. On the other hand, printed layers must harden quickly to support the superposed layers. Another important inherent aspect of 3D printing is inter-layer bonding. Due to the lack of vibration or external force during deposition,

© RILEM 2019
T. Wangler and R. J. Flatt (Eds.): DC 2018, RILEM Bookseries 19, pp. 234–244, 2019.
https://doi.org/10.1007/978-3-319-99519-9_22

layers must bond in an optimal way in order to create a homogeneous structure and provide adequate mechanical strength. The layered manufacturing process will also include voids in the specimen. These voids will create weak links in the interface behavior and will not only affect the mechanical behavior but also the durability as these voids are ideal ingress paths for chemical substances.

2 Materials and Methods

2.1 Materials and Mix Composition

Ordinary Portland cement (CEM I 52.5 N) was combined with standardized sand with a maximum particle size equal to 2 mm. To increase the flowability of the cementitious mixture, a polycarboxylic ether (PCE) with a molecular weight of approximately 4000 g/mol and 35% solids was used as a superplasticizer. The mix composition can be found in Table 1.

Table 1. Mix composition

Material [-]	Amount [g]
CEM I 52.5 N	675
Sand	1350
Water	246
PCE	0.26% [weight of cement]

The mix design aimed to meet 3D printing requirements, including extrudability, buildability and workability. To classify the composition as extrudable, two demands have to be fulfilled. First, the extrudability was tested by filling the 3D print apparatus and extruding one layer with a length of 300 mm. Once the mortar was expelled without blocking, segregation or bleeding, the mix composition met the first requirement. Second, the deformation of the layer after extrusion was considered. Deformations within a range of 10% were excepted. Buildability was obtained when different layers of material could be printed on top of each other and a general conclusion about the workability was made by performing Vicat tests (manual and automatic). These tests not only evaluate the yield stress of the material but also the buildup capacity as a function of time.

2.2 3D Printing Process

3D Printing Apparatus

A custom-made apparatus was used to simulate an extrusion-based 3D printing process (Fig. 1). The developed system is capable of printing up to 300 mm long concrete layers, at different speeds and different deposition rates. The nozzle of the print equipment has an elliptical shape (28 mm × 18 mm). The height of each layer is equal to 10 mm with an average layer width of 30 mm. For the purpose of this study, linear

printing speeds of 1.7 cm/s and 3 cm/s were selected. The effect of a changing pressure inside the nozzle, accompanied with the different printing speeds, was not taken into account in this research.

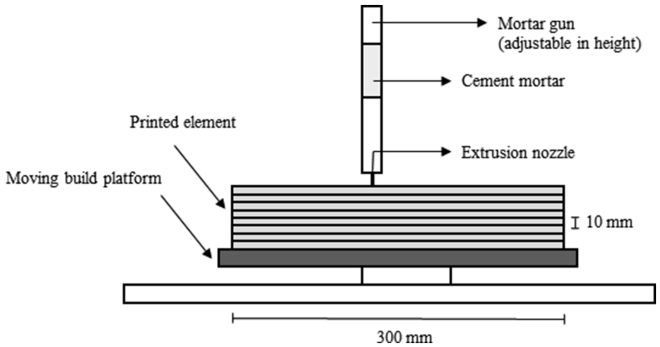

Fig. 1. Schematic illustration of the extrusion-based 3D printing process

Specimen Preparation

Sample preparation consists of filling the 3D printing apparatus and extruding material through the nozzle with a constant speed (1.7 cm/s and 3 cm/s). A single base layer, with a length of approximately 300 mm, was extruded for each specimen. After a predetermined time interval (0, 10 or 60 min), another layer was deposited on top of the previous one. In case of a zero time gap, the two layers were printed form the same batch of material. After 5 min, the material was difficult to print and therefore a fresh mortar mix was deposited on the first layer with 10 and 60 min time gap intervals. All the specimens were cured in a standardized environment (20 ± 3 °C) until the day of testing (i.e. 28 days after printing).

2.3 Surface Roughness

The surface roughness of the printed specimens was determined by the in house developed Automated Laser Measurement (ALM) technique, scanning the surface of the layers with a high precision beam, equipped with two stepping motors controlling the motion in X and Y direction. The profile measurements are used to calculate the center-line roughness (R_a) value of the printed specimens. This value is determined with an average line drawn through the profile and the center-line over a selected reference length (200 mm in Y-direction, 15 mm in X-direction), selected to include important roughness features, but exclude errors of form. Using the ALM, the R_a value can be derived with an accuracy of 7 μm. The surface roughness was measured every 5 and 50 mm in respectively X and Y direction (Fig. 2). Roughness measurements were performed for every printing speed.

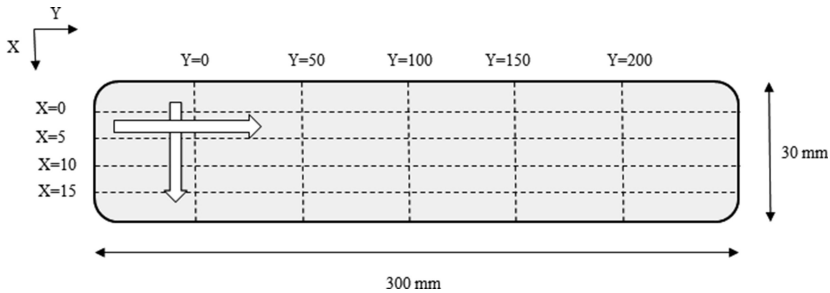

Fig. 2. Schematic representation of the surface roughness measurement (ALM)

2.4 Mechanical Properties Testing

Compressive Strength

The compressive strength of the specimens was tested in a universal testing machine under load control at a rate of 100 N/sec and is schematically illustrated in Figs. 3 and 4. For the compressive strength test, small cylinders were saw-cut from the printed elements with a height and diameter respectively equal to 20 and 25 mm. The specimens were loaded perpendicular to the print direction. At least 3 specimens were tested for every time gap and printing speed.

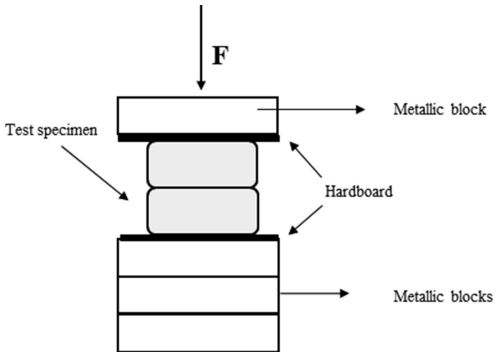

Fig. 3. Schematic illustration of the compressive strength test setup

Inter-layer Bonding Strength

The schematic illustration of the inter-layer bonding strength test setup is shown in Fig. 5. The test specimens were small cylinders, saw-cut from the original printed elements, with a height and diameter respectively equal to 20 and 25 mm. These specimens have analogue dimensions as the ones used for testing the compressive strength (Fig. 4). Two metallic brackets were epoxy glued on the top and bottom of the printed specimens. The inter-layer bonding strength test was conducted in an universal testing machine under displacement control at the rate of 50 N/s. Special attention was taken to align the specimens in order to avoid any eccentricity. At least 3 specimens were tested for every time gap and printing speed.

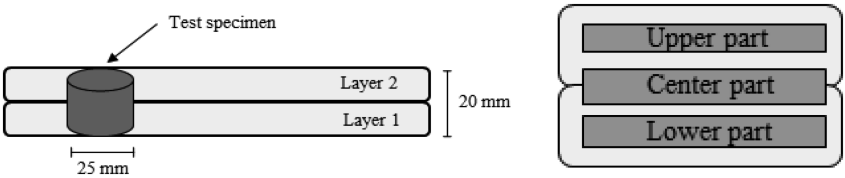

Fig. 4. Schematic illustration of sampling elements (left) and indication of the different zones in a printed element (right)

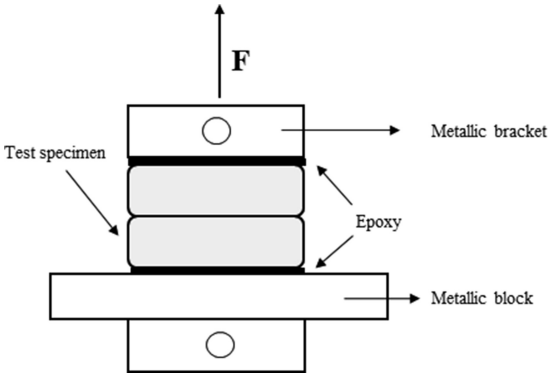

Fig. 5. Schematic illustration of the inter-layer bonding test setup

2.5 Porosity Measurements and Pore Size Distribution

Porosity tests were conducted on small cylinders, saw-cut from the original printed elements, with a height and diameter respectively equal to 20 and 14 mm (Fig. 4). The cylindrical elements were dried in an oven at 35 °C until constant weight. The weight of the samples at this stage is designated as dry weight and indicated as m_1 [g]. Thereafter, the samples were submerged in water with a temperature of 20 °C until complete saturation. The weight of the samples in soaked water was measured (m_2 [g]), followed by rolling the different sides on a damp cloth measured as m_3 [g]. From this, the apparent porosity (P_a) of the samples was calculated using Eq. (1).

$$P_a = (m_3 - m_1)/(m_3 - m_2) \cdot 100 \quad (1)$$

To measure the pore sizes and pore size distribution, Mercury Intrusion Porosimetry (MIP) was used. As a specific pressure corresponds to an aperture of a pore, and the amount of mercury intrusion approximates to the pores volume, the amount and size of the pores can be determined. MIP is performed for every series on samples taken from the upper, lower and center region after freeze-drying the samples for 7 days.

3 Results and Discussion

3.1 Surface Roughness

Table 1 gives an overview of the R_a-values of the printed specimens. The results in x-direction show the average values of 5 measurements, in y-direction 4 measurements on different positions were performed. One can see that the applied printing speed has a significant influence on the surface roughness. A lower speed introduces a higher roughness, which will have a positive effect on the mechanical properties, as can be seen in Sects. 3.2 and 3.3. In case of a lower printing speed, the surface roughness is more pronounced in X-direction. For the higher printing speed, the roughness values are more or less the same in both directions. This will also affect the anisotropic behavior of the printed elements, but these results are not included in this paper.

3.2 Compressive Strength

Figure 6 presents the compressive strength and associated standard deviation for a mixture printed with different speeds and different time gaps. One can see that the compressive strength decreases when increasing the time gap and the overall strength of the specimens is higher when printing on a lower speed. Table 2 also indicates the strength loss due to a layered manufacturing process. This loss is given as the ratio of 'difference in compressive strength with certain time gap' to the compressive strength of the basis one without time gap between the layers (Eq. (2)).

$$\Delta = \frac{\text{Strength}_0 - \text{Strength}_{\text{time gap}}}{\text{Strength}_0} \tag{2}$$

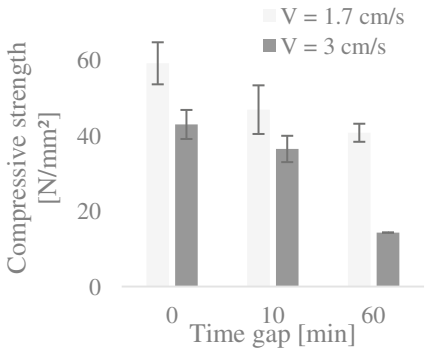

Fig. 6. Compressive strength

Table 2. Average roughness R_a of elements fabricated with different printing speeds

Printing speed [cm/s]	$R_{a,x}$ [mm]	stdev [-]	$R_{a,y}$ [mm]	stdev [-]
1.7	0.95	0.05	0.68	0.15
3	0.39	0.07	0.46	0.08

3.3 Inter-layer Bonding Strength

Figure 7 presents the inter-layer bonding strength and associated standard deviation for the different elements. For every printing speed, the interlayer bonding decreases when increasing the time gap and the overall strength of the printed specimens is higher in case of a lower speed. As indicated in literature [1, 3, 4], the inter-layer bonding strength between two different layers is related to the surface roughness. Due to the lower roughness in case of higher speed, the bonding between the layers decreases. Based on the results of Table 3, one can conclude that there is almost no bonding between the layers printed with a time gap of 60 min. The formation of this cold joint can be explained by a moisture exchange phenomenon that states, when the bottom layer becomes drier, it absorbs more water from the freshly deposited top layer and simultaneously, some air inside the bottom layer escapes out of it. This air stays entrapped at the interface and causes poor bonding [2]. Table 3 also indicates the strength loss due to a layered manufacturing process and this is again higher in case of a higher printing speed (Table 4).

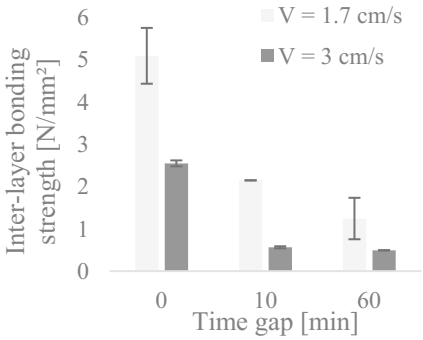

Fig. 7. Inter-layer bonding strength

Table 3. Compressive strength

Time gap [min]	F [N/mm^2]	stdev [-]	Loss Δ [%]
V = 1.7 cm/s			
0	59.21	5.58	-
10	46.92	6.45	20.77
60	40.79	2.40	31.12
V = 3 cm/s			
0	42.99	3.85	
10	36.49	3.50	15.12
60	14.29	-	66.75

Table 4. Inter-layer bonding strength

Time gap [min]	F [N/mm^2]	stdev [-]	Loss Δ [%]
V = 1.7 cm/s			
0	5.08	0.66	
10	2.14	-	57.51
60	1.24	0.49	75.43
V = 3 cm/s			
0	2.54	0.07	
10	0.56	0.02	88.87
60	0.49	-	96.53

3.4 Microstructure and Porosity

Based on Fig. 8A, it becomes clear that comparing different parts of a printed element with a time gap equal to zero, the pore size distribution is comparable for every region. This in contrast to what is obtained for elements with a 10 min time gap, where the amount of pores with a specific diameter is higher in the center and lower part of the layer (Fig. 8B). This probably indicates that printing a second layer will compact the layer underneath when printing without a time gap. In case of a time gap equal to 10 min, the first layer is already hardened to some extent and less affected by compaction due to printing the second layer. The same conclusion can be made for a time gap of 60 min (Fig. 8C). Figures 8D–F show a comparison between the different parts of a printed element, fabricated with different time gaps. Comparing the upper part, one can only see a shift towards bigger pores in case of a time gap equal to 10 or 60 min. The amount of pores is more or less the same. In case of the center and lower part of the specimens, there is not only a shift towards bigger pores but also the amount of pores increases significantly compared to a specimen fabricated without time gap. This can again be explained by a moisture exchange phenomenon where a drier bottom layer absorbs more water from the super positioned fresh layer and simultaneously, some air inside the bottom layer escapes out of it and will induce bigger pores in the lower and center part of the specimen. The same conclusions can be made for a higher printing speed. These graphs are not included in this paper.

Figure 9 shows a comparison between the pore size distribution of an upper part element, printed with a time gap equal to zero, for different printing speeds. One can see clear that printing on a higher speed will induce a higher amount of bigger pores in the system, what will have a negative effect on the durability of the material. Consequently, further research on this topic is mandatory.

Mercury Intrusion Porosimetry makes it possible to measure pores ranging from 0.005 μm to 10 μm. These pores are capillary pores and are formed during the hydration process of cement. The capillary pores will describe the microstructure of the element and are mainly affected by the amount of cement, the water/cement ratio and

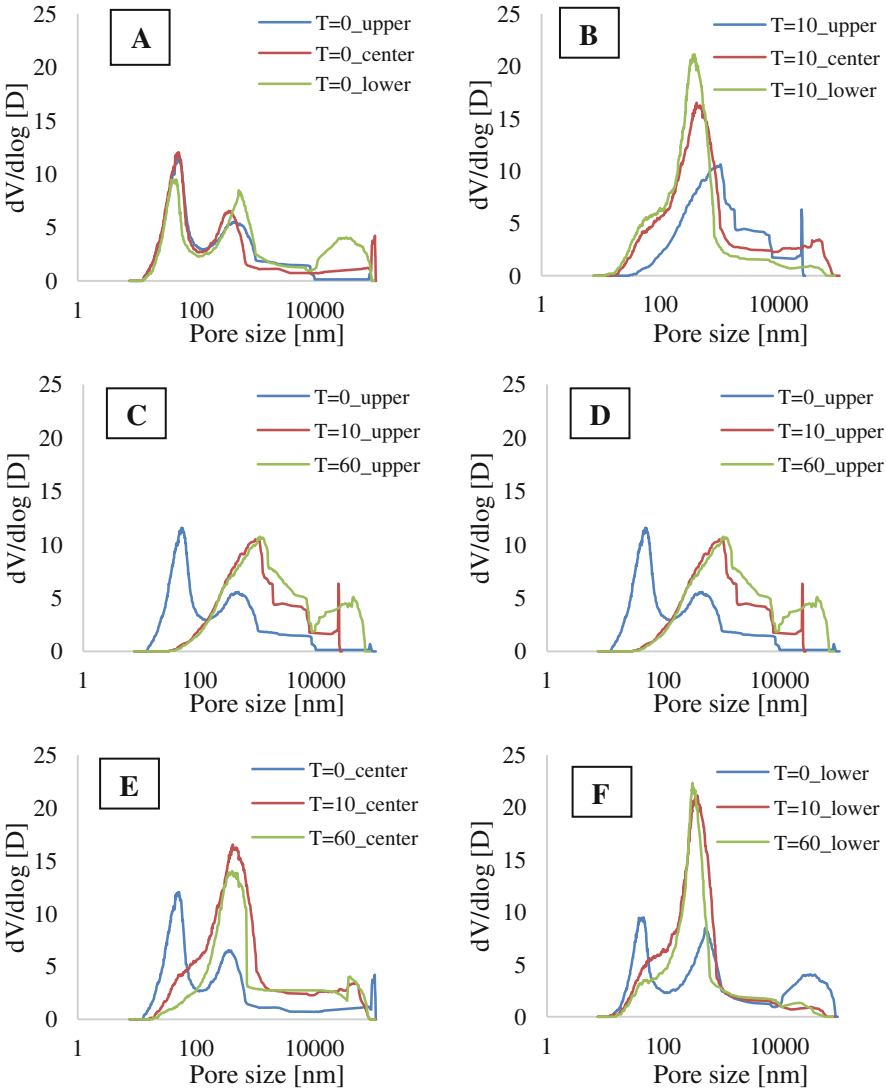

Fig. 8. Pore size distribution of elements with different time gaps and low printing speed

the degree of hydration [5]. Another type of porosity is the open porosity. These results are given by Fig. 10. Open porosity defines the pores on the outside of the printed elements. Here a decreasing trend is visible when increasing the time gap between the different layers. One can also see that in case of a high printing speed, the porosity is less affected.

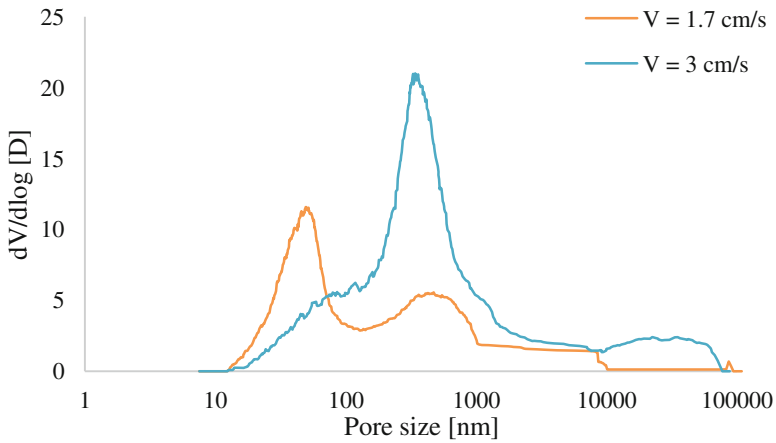

Fig. 9. Pore size distribution of the upper region in case of two different printing speeds

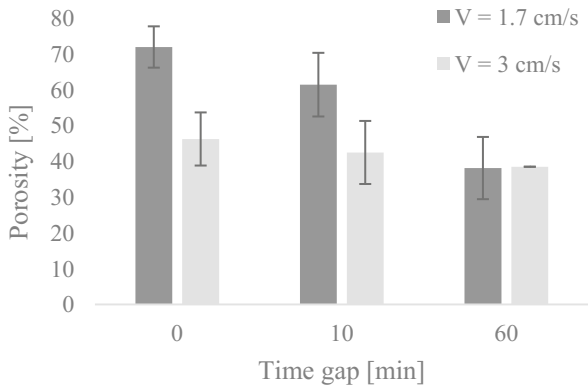

Fig. 10. Open porosity of printed elements fabricated with different speeds

4 Conclusions

The effects of different delay times and a changing print speed on the mechanical properties and the (micro)structure of 3D printed elements were investigated in this research. The mix composition was kept the same during all the experiments. The following conclusions can be drawn from this study:

1. The surface roughness of specimens fabricated with a higher printing speed was lower compared to the ones printed with a lower speed. There was a significant difference in roughness between the X- and Y- direction in case of a low printing speed. The difference in roughness was less pronounced for a higher printing speed.

2. The compressive strength and the inter-layer bonding strength of the elements was higher when fabricating the elements on a low speed and in case there was no time gap between the different layers.
3. Increasing the delay time induces a higher amount of bigger pores in the lower and center part of the printed specimens.
4. Increasing the printing speed introduces bigger pores. This not only affects the mechanical properties, but also the durability of the material.

Acknowledgements. The authors would like to acknowledge the support by EFRO for this C3PO-project with a total amount of € 668 320.41.

References

1. Zareiyan, B., Khoshnevis, B.: Interlayer adhesion and strength of structures in contour crafting: effects of aggregate size, extrusion rate, and layer thickness. Autom. Constr. **81**, 112–121 (2017)
2. Panda, B., et al.: Measurement of tensile bond strength of 3D printed geopolymer mortar. Measurement **113**, 108–116 (2018)
3. Zareiyan, B., Khoshnevis, B.: Effects of interlocking on interlayer adhesion and strength of structures in 3D printing of concrete. Autom. Constr. **83**, 212–221 (2017)
4. Eduardo Nuno Brito Santos, P.M.D., Eduardo, J.: Factors affecting bond between new and old concrete. Mater. J. **108**(4), 449–456 (2011)
5. Boel, V.: Microstructuur van zelfverdichtend beton in relatie met gaspermeabiliteit en duurzaamheidsaspecten, p. 320. Ph.D. dissertation, University of Ghent (2007)